Grid-Aware Hierarchical MPC Framework for Colocated Electric Vehicle Charging Stations Coordination

Ahmed S. Abdelaal and Ramadan ElShatshat
Department of Electrical and Computer Engineering University of Waterloo, Waterloo, ON, Canada

***Abstract*—This paper presents a grid-aware two-layer hierarchical model predictive control (MPC) framework for real-time coordination of colocated electric vehicle charging stations (EVCSs) on distribution networks. The proposed framework uniquely combines a neural state-space model (NSSM) for high-fidelity feeder dynamic representation with a proportional load-sharing mechanism that equitably distributes available feeder import capacity among colocated EVCSs. At the upper layer, the MPC integrates the NSSM into an optimal power flow (OPF) problem to enforce voltage and thermal constraints while minimizing system operational costs. It dynamically allocates the feeder's remaining thermal margin in proportion to the charging energy demand at each EVCS, ensuring fairness and preventing localized congestion. At the lower layer, independent MPCs optimize local EV charging schedules using photovoltaic (PV) generation, battery energy storage (BESS), and time-of-use (TOU) pricing, maintaining user satisfaction and privacy without centralized data exchange. Simulations on the IEEE 69-bus feeder under stochastic EV behavior show 34% feeder-peak and 70% station-peak reductions, maintaining voltage and thermal compliance. This approach effectively bridges centralized and distributed coordination paradigms, achieving scalable, privacy-preserving, and grid-compliant operation suitable for high EV penetration scenarios.**

***Index Terms*—Electric Vehicles Charging, Hierarchical MPC, Neural State-Space Model, Load Sharing, Distribution System Coordination, Grid-Aware Control**

I. Introduction

The rapid growth of electric vehicles (EVs) adaptation has introduced clustered, high-power, and time synchronous charging loads that impose significant operational stress on distribution feeders not originally designed for such dynamics. Uncoordinated EV charging can cause voltage deviations, feeder congestion, and thermal overloading, particularly in low-voltage feeders where local peaks can propagate upstream, accelerating asset degradation.

Existing centralized model predictive control (MPC) schemes offer effective scheduling capabilities to mitigate congestion and optimize operational costs [1], [2]. However, they require complete system observability and user-level data, such as arrival times, departure schedule, and SOC information raising scalability and privacy concerns [3]. Alternatively, price-based demand management schemes, including time-of-use (TOU) and real-time pricing, have been adopted to influence charging behavior. Yet, these methods lack real-time feedback and may unintentionally create secondary demand peaks by synchronizing user response to low-price periods, causing localized congestion and voltage violations [4], [5].

Distributed and hierarchical MPC frameworks have emerged as promising alternatives that balance grid-level coordination with user privacy, enabling localized decision-making with limited data exchange [1]–[3], [6]. However, many existing distributed MPC schemes rely on linearized power-flow models or deterministic forecasts of renewable generation and EV demand, limiting their accuracy and robustness under stochastic operating conditions. Distributed consensus and energy-sharing methods also demonstrate that cooperative strategies can balance feeder imports and improve resource utilization while maintaining privacy [5], [7]. Yet, these approaches primarily address energy sharing or cost minimization, rather than enforcing feeder thermal and voltage constraints. In addition, only a small number of studies consider colocated EV charging stations (EVCSs), and even fewer ensure that combined EV charging and native feeder loads remain within thermal limits under uncertain EV arrivals. Overall, existing approaches lack full grid awareness and do not guarantee fair, capacity-constrained allocation of feeder import capability among colocated EVCSs even in frameworks employing quota-based coordination [8], capacity signaling [4], or robust uncertainty handling [3].

To address these limitations, this paper introduces a grid-aware hierarchical MPC framework for coordinating colocated EVCSs in real-time. The proposed approach uniquely integrates a neural state-space model (NSSM) to capture nonlinear feeder dynamics with a proportional load-sharing mechanism that equitably distributes the available feeder import capacity among colocated EVCSs. The upper-layer MPC (UL-MPC) performs optimal power flow (OPF) to enforce voltage and thermal constraints while minimizing operational costs. It dynamically determines the remaining feeder capacity and allocates it proportionally to each colocated EVCS based on the energy demand, ensuring fairness and preventing localized overloads. Each lower-layer MPC (LL-MPC) operates autonomously at the EVCS level, optimizing charging schedules to minimize cost and meet user SOC targets while leveraging local resources such as photovoltaic (PV) generation, battery energy storage systems (BESS), and TOU pricing signals. This hierarchical structure combines the accuracy and grid fidelity of centralized MPC with the privacy, scalability, and autonomy of distributed control. It enables real-time operation under stochastic EV

979-8-3315-8138-1

behavior without requiring global data sharing, making it suitable for future large-scale EV integration scenarios.

The main contributions of this work are summarized as follows:

- Neural State-Space MPC: An MPC that ensures grid-aware coordination between colocated EVCSs, and employs a data-driven NSSM to capture nonlinear feeder dynamics.
- Fair Load Sharing: Introduces a proportional feeder-capacity allocation mechanism based on individual and aggregate charging energy demand of connected EVs.
- Scalable, Privacy-Preserving Control: Employs decentralized MPCs using PV, BESS, and TOU inputs, achieving up to 34% feeder-peak and 70% station-peak reductions with full grid voltage and feeder thermal compliance.

The remainder of the paper is organized as follows. Section II presents the proposed hierarchical MPC methodology, including the UL-MPC and LL-MPC formulations. Section III discusses the simulation setup and results using the IEEE 69-bus feeder. Section IV concludes the paper with key findings and implications for grid-aware EV integration.

II. METHODOLOGY

A. Upper Layer MPC: Grid-Aware Load Sharing and EVCS Coordination

The proposed hierarchical MPC framework for coordinating colocated EVCSs is shown in Figure 1. The two-layer structure includes a UL-MPC for grid level coordination, which uses an NSSM to capture the nonlinear dynamics of the distribution system for efficient, high-fidelity voltage estimation [9]. The UL-MPC solves OPF, incorporating forecasts of renewable energy resources (RES), and base load, while enforcing voltage and thermal limits and minimizing total operational cost. LL-MPCs at each EVCS receive a permitted grid power imports signal, dependent on the available line capacity and the energy required to charge the connected EVs, from the UL-MPC and autonomously schedule individual EV charging to meet user objectives.

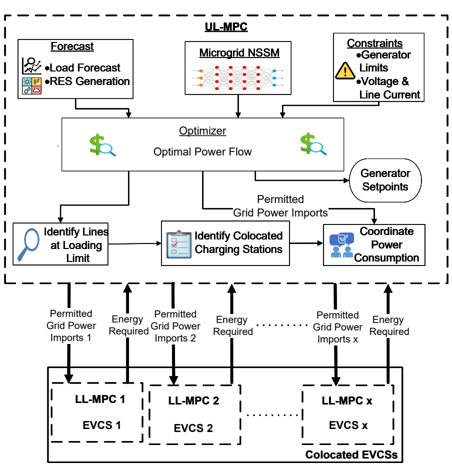

Fig. 1: UL-MPC architecture for grid-aware load sharing and coordinaton of colocated EVCSs.

The objective function of the UL-MPC is expressed in (1a)-(1d), where the total cost is the sum of the fuel, wind, and PV operation and maintenance (O&M) costs over the number of generators N_G over the total duration T. The fuel cost, shown in (1b), is modeled as a quadratic function of generator output, with a_i, b_i, and c_i denoting cost coefficients, c_i^{fuel} the fuel energy cost ($/kWh) for the time duration τ, and the generated power at bus i and time step t, $P_{i,t}^G$. The O&M costs for wind and PV generation are given by (1c) and (1d), where $P_{i,t}^{\text{wind}}$ and $P_{i,t}^{\text{PV}}$ denote the respective power outputs, and c^{wind} and c^{PV} represent the energy cost. Power balance at all buses n, is enforced through (1e) and (1f), which ensure that total real and reactive $Q_{i,t}^G$ power generation and renewable powers equals the real $P_{i,t}^D$ and reactive $Q_{i,t}^D$ demand. Here, G_{ik} and B_{ik} represent the real and imaginary parts of the bus admittance matrix between buses i and k, δ_{ik} is the voltage angle difference, and $|V_{i,t}|$ denotes the voltage magnitude at bus i.

$$\min J = \sum_{t=1}^{T}\sum_{i=1}^{N_G}\left(\mathrm{C}_{i,t}^{\text{fuel}} + C_{i,t}^{\text{wind,O\&M}} + C_{i,t}^{\text{PV,O\&M}}\right) \tag{1a}$$

$$\mathrm{C}_{i,t}^{\text{fuel}} = c_i^{\text{fuel}} \cdot \left(c_i + b_i \cdot P_{i,t}^{\mathrm{G}} + a_i \cdot \left(P_{i,t}^{\mathrm{G}}\right)^2\right) \cdot \tau \tag{1b}$$

$$C_{i,t}^{\text{wind,O\&M}} = c^{\text{wind}} \cdot P_{i,t}^{\text{wind}} \cdot \tau \tag{1c}$$

$$C_{i,t}^{\text{PV,O\&M}} = c^{\text{PV}} \cdot P_{i,t}^{\text{PV}} \cdot \tau \tag{1d}$$

Subject to:

$$\sum_{k=1}^{n} |V_{i,t}||V_{k,t}|\big(G_{ik}\cos\delta_{ik} + B_{ik}\sin\delta_{ik}\big) = P_{i,t}^G + P_{i,t}^{\text{wind}} + P_{i,t}^{\text{PV}} - P_{i,t}^{\text{D}} \tag{1e}$$

$$\sum_{k=1}^{n} |V_{i,t}||V_{k,t}|\big(G_{ik}\sin\delta_{ik} - B_{ik}\cos\delta_{ik}\big) = Q_{i,t}^G - Q_{i,t}^{\text{D}} \tag{1f}$$

$$P_i^{\min} \le P_{i,t}^G \le P_i^{\max} \tag{1g}$$

$$Q_i^{\min} \le Q_{i,t}^G \le Q_i^{\max} \tag{1h}$$

$$P_{ij,t} \le P_{ij}^{\max} \tag{1i}$$

$$V_i^{\min} \le |V_{i,t}| \le V_i^{\max} \tag{1j}$$

$$A_{ij,t} = P_{ij}^{\max} - P_{ij,t} \tag{1k}$$

$$E_{\mathcal{X}_{ij},t} = \sum_{x\in\mathcal{X}_{ij}} e_{x,t} \quad x \in \mathcal{X}_{ij} \tag{1l}$$

$$P_{x,t}^{permitted} = P_{x,t}^{EVCS,load} + A_{ij,t} \cdot \frac{e_{x,t}}{\max\{1,\, E_{\mathcal{X}_{ij},t}\}} \tag{1m}$$

The operational constraints of the distribution feeder are expressed in (1g)–(1j), which limit generator real and reactive power output, $P_{ij,t}$ the real power flow on line ij, and voltage magnitudes within their permissible ranges. The available line capacity is computed in (1k) which represents the remaining real power flow margin to the thermal limit $P_{ij}^{\max}$ on line ij.

979-8-3315-8138-1

To distribute this available capacity fairly among colocated EVCS connected to line ij, the UL-MPC first determines the total energy required to charge all the vehicles at the colocated EVCSs using (1l), where $e_{x,t}$ is the energy required to charge the vehicles at EVCS x and $\mathcal{X}_{ij}$ is the set of colocated EVCSs fed from line ij. The UL-MPC then allocates the permitted grid imports $P_{x,t}^{permitted}$ to each LL-MPC situated at the EVCS x, through proportional load sharing in (1m), where $P_{x,t}^{EVCS,load}$ is the EVCS's current load and $\max\{1,\, E_{\mathcal{X}_{ij},t}\}$ evades division by zero. This ensures that aggregate imports across colocated EVCSs remain within line capacity, maintaining fairness, preventing localized overloads, and adapting dynamically to varying EV arrivals and departures. Once these limits are communicated, the LL-MPCs operate autonomously to allocate charging power among individual EVs while ensuring that the consumption of the EVCS remains within its assigned permitted grid power imports.

B. Lower Layer MPC: Grid-Aware Coordinated Charging

Figure 2 illustrates the LL-MPC at each EVCS, which schedules individual EV charging to meet user objectives while respecting UL-MPC imposed limits. Each controller leverages local PV generation, BESS flexibility, and charger ratings, relying solely on local measurements to preserve user privacy, and enable real-time scalability across multiple colocated EVCSs. The LL-MPC formulation is given in (2a)-(2l). The objective function in (2a) minimizes the total energy cost, which consists of two main components. The first component is the cost of EV charging across all Y vehicles and the second component is the cost of power consumed by the BESS. The TOU electricity price, TOU_t, was obtained from the Ontario Energy Board [10]. The variables $P_{y,t}^{EV}$ and P_t^{BESS} denote the charging power of EV y and the BESS at time step t, and τ represents the time duration. The equivalent stored energy for each EV and the BESS is described in (2b) and (2c), where $SOC_{y,t}^{EV}$ and SOC_t^{BESS} are the respective states of charge, and $E_y^{EV,cap}$ and $E^{\text{BESS},cap}$ denote the total energy capacities.

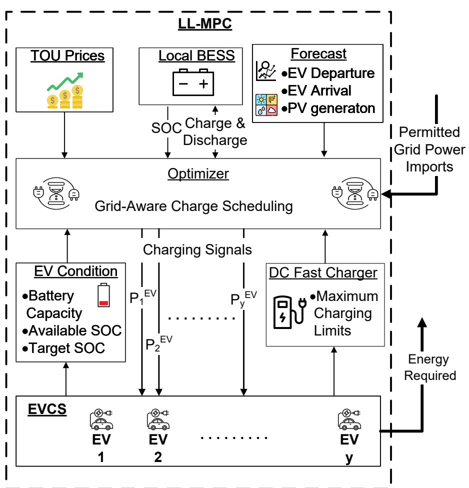

Fig. 2: LL-MPC architecture for grid-aware EV charging at a single EVCS.

The energy dynamics of each EV battery are given by (2d), where $\eta_y^{EV,ch}$ is the charging efficiency. Similarly, the BESS energy update in (2e) captures both charging and discharging processes, with efficiencies $\eta^{\text{BESS},ch}$ and $\eta^{\text{BESS},dis}$, respectively. The magnitude of P_t^{BESS} corresponds to $P_t^{\text{BESS},ch}$ when positive and $P_t^{\text{BESS},dis}$ when negative. The operational constraints of the LL-MPC are defined in (2f)–(2l). Each EV y is only permitted to charge within its connection window $[T_y^{\text{arr}}, T_y^{\text{dep}}]$ as enforced by (2f) and (2g), where the upper limit $P^{\text{charger,max}}$ depends on the charger rating.

$$\min J = \sum_{t=1}^{T} \tau \left(\sum_{y=1}^{Y} TOU_t \cdot P_{y,t}^{EV} + TOU_t \cdot P_t^{\text{BESS}} \right) \tag{2a}$$

$$E_{y,t}^{EV} = SOC_{y,t}^{EV} \cdot E_y^{EV,cap} \tag{2b}$$

$$E_t^{\text{BESS}} = SOC_t^{\text{BESS}} \cdot E^{\text{BESS},cap} \tag{2c}$$

$$E_{y,t}^{EV} = E_{y,t-1}^{EV} + \eta_y^{EV,ch} \cdot P_{y,t}^{EV} \cdot \tau \tag{2d}$$

$$E_t^{\text{BESS}} = E_{t-1}^{\text{BESS}} + \left(\eta^{\text{BESS},ch} \cdot P_t^{\text{BESS},ch} - \frac{P_t^{\text{BESS},dis}}{\eta^{\text{BESS},dis}} \right) \cdot \tau \tag{2e}$$

Subject to:

$$0 \le P_{y,t}^{EV} \le P^{charger,\max} \quad \forall t \in [T_y^{\text{arr}}, T_y^{\text{dep}}] \tag{2f}$$

$$P_{y,t}^{EV} = 0 \quad t < T_y^{\text{arr}}, t > T_y^{\text{dep}} \tag{2g}$$

$$|P_t^{\text{BESS}}| \le P^{charger,\max} \tag{2h}$$

$$SOC_{y,t}^{EV} = SOC_y^{EV,target} \quad \forall t = T_y^{\text{dep}} \tag{2i}$$

$$SOC^{EV,\min} \le SOC_{y,t}^{EV} \le SOC^{EV,\max} \tag{2j}$$

$$SOC^{\text{BESS},\min} \le SOC_t^{\text{BESS}} \le SOC^{\text{BESS},\max} \tag{2k}$$

$$\sum_{y=1}^{Y} P_{y,t}^{EV} + P_t^{\text{BESS}} - P_t^{PV} \le P_t^{permitted} \le P^{EVCS,cap} \tag{2l}$$

The BESS power constraint (2h) limits its charging and discharging within its rated power capacity. Equation (2i) ensures that every EV reaches its target SOC, $SOC_y^{EV,target}$, at its departure time T_y^{dep}, while (2j) and (2k) maintain the SOC levels of both EVs and the BESS within safe operating bounds. Finally, the feeder power constraint in (2l) guarantees that the EVCS load represented by the total instantaneous charging demand from all EVs, combined with BESS power exchange, and local PV generation P_t^{PV}, does not exceed either the permitted grid import limit $P_t^{permitted}$ or the physical capacity of the EVCS, $P^{EVCS,cap}$.

The LL-MPCs operate concurrently with the UL-MPC to achieve real-time, grid-aware coordination. At each interval, the UL-MPC updates the permitted grid import $P_t^{permitted}$ based on feeder conditions, while each LL-MPC optimizes local charging within these limits. This hierarchical structure preserves privacy, leverages local PV and BESS resources, and ensures scalable, cost-effective, and grid-compliant EV charging under dynamic conditions.

979-8-3315-8138-1

III. Results & Discussions

A. System Description

The framework was validated on the IEEE 69-bus test feeder which operates at 12.66 kV with maximum real and reactive demands of 3800 kW and 2690 kVAR, respectively. The daily load profile in Figure 3 follows a typical pattern, increasing through the morning, peaking around mid-day, and subsiding in the evening. Three 1500 kVA generators were installed at buses 3, 7, and 61 using cost parameters from [9]. Distributed resources include 250 kW wind farms at buses 27, 35, 46, and 65, and 100 kW PV farms at buses 50, 52, 67, and 69. Three colocated 350 kW EVCSs, each equipped with 50 kW DC fast chargers [11], were connected to bus 48 and are supplied by the feeder between buses 4-47 (Line 4-47). Each EVCS also integrates a 20 kW local PV array and a 50 kWh BESS to support local energy management. The UL-MPC uses renewable forecasts generated from statistical weather-driven models, with solar irradiance modeled by a Beta PDF and wind speed by a Weibull PDF. The parameters $(\alpha = 3, \beta = 10)$ and $(k = 2, c = 9)$, respectively, were derived from historical data, and PV and wind power outputs were computed following the methodology in [12]. Stochastic EV user behavior is captured via Monte Carlo simulations with 1000 daily scenarios, modeling random arrival times and initial SOC using lognormal distributions with parameters $(\mu = 1.3, \sigma = 0.8)$ and $(\mu = 0.35, \sigma = 0.1)$, respectively [13].

An NSSM was employed for voltage estimation following [9], using 40,000 samples for training and validation. The model achieved a mean-squared error of 0.012 and a validation accuracy of 99.3%. Figure 4 shows the maximum voltage magnitude error between NSSM predictions and AC power flow solutions across all buses, with a worst-case deviation below 0.8%. Figure 5 illustrates feeder-wide voltage variation over the day, where the maximum deviation is 4.6% at bus 48, remaining within the 5% voltage limit. This level of accuracy is sufficient to preserve model fidelity and ensure reliable constraint enforcement.

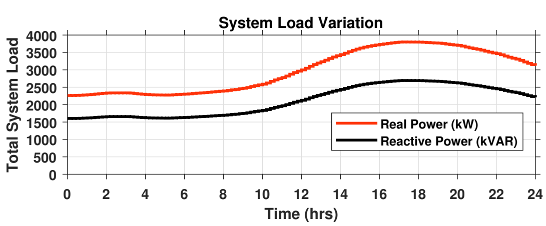

Fig. 3: IEEE 69-bus test feeder load variation throughout the day.

B. Grid-Aware Hierarchical MPC for Colocated EVCS Charging

Figure 6 illustrates the real power flow on line 4-47 under three operating conditions: base case (no EVCSs), grid-unaware and grid-aware coordination (with 3 EVCS). No thermal limit violations were observed on any other lines in the system. In the base case, the feeder peak load reached 1035 kW at 17 hrs, remaining below the 1100 kW thermal limit. With three

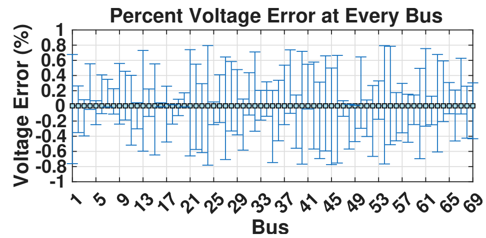

Fig. 4: NSSM voltage error with respect to AC power flow.

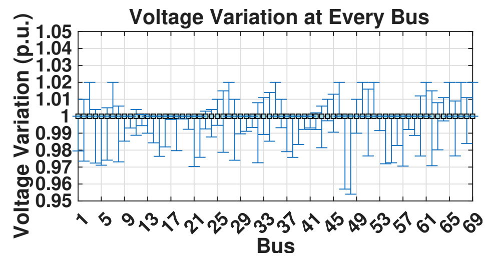

Fig. 5: Voltage variation throughout the day.

colocated EVCSs connected, uncoordinated charging increased line 4-47 loading to 1665 kW at 16 hrs, and exceeded the thermal limit for approximately two hours (16-18 hrs). Such overloading accelerates thermal aging and may compromise asset lifespan. Under grid-aware coordination, the UL-MPC enforced a 1100 kW limit on the feeder by adjusting the permitted grid imports for each EVCS. The resulting power flow curve was flattened, maintaining operation at the thermal limit between 13-18 hrs. This reduced the peak feeder load by nearly 34% and distributed the charging activity over a longer period, demonstrating effective load shaping and feeder protection. Figures 7a–7c show the impact of grid awareness on the load profiles of the colocated EVCSs. EVCS 1, 2, and 3 reached peak loads of 350, 350, and 132 kW at 16, 16, and 13 hrs for the grid-unaware operation and 111, 102, and 102 kW at 13.5, 14.5, and 11.5 hrs for grid-aware coordination respectively. In addition, the reductions in peak load were 68%, 70%, and 22% with charging spread over a longer interval. The peaks that occur in the grid-unaware operation correspond to high TOU prices, illustrating how price-based control alone can inadvertently shift congestion rather than alleviate it. In contrast, the proposed hierarchical MPC reshaped the temporal charging distribution, maintaining operation within the permitted imports computed by the UL-MPC.

The grid-aware hierarchical coordination effectively distributed feeder capacity among colocated EVCSs through the permitted grid power imports signal, ensuring fair load sharing and compliance with voltage and thermal constraints. By directing each LL-MPC to adapt charging schedules in real-time, the UL-MPC prevented overlapping peaks and alleviated feeder congestion. The LL-MPCs utilized local PV and BESS resources to meet charging objectives within their assigned permitted grid power import limit, reducing reliance on the main feeder while maintaining user SOC targets and deadlines. Overall, the proposed framework achieved robust, privacy-preserving coordination under stochastic EV behavior, mitigating peak demand, improving feeder thermal utilization, and ensuring equitable power allocation across colocated EVCSs without centralized data exchange. These results confirm that grid-aware hierarchical control enhances operational reliability and scalability for high EV penetration in distribution networks.

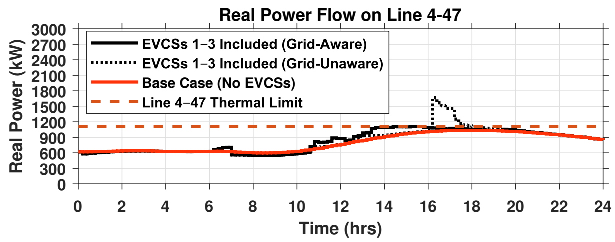

Fig. 6: Real power flow on line 4-47 under grid-aware and grid-unaware operations compared with the line thermal limit.

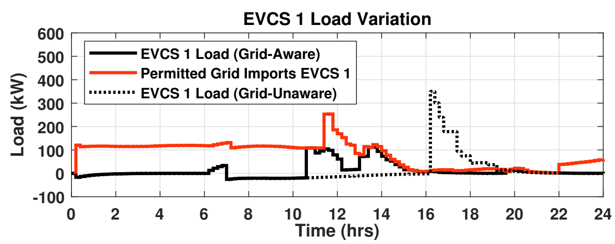

(a)

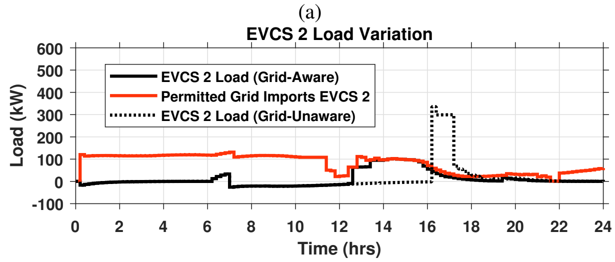

(b)

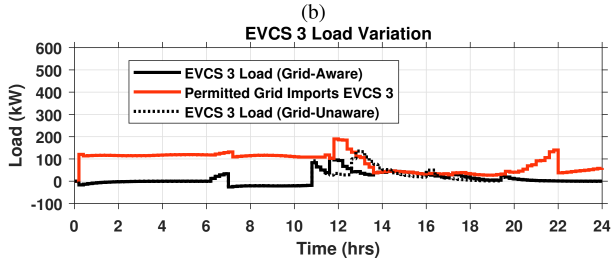

(c)

Fig. 7: Load profile under grid-aware and grid-unaware operations for (a) EVCS 1 (b) EVCS 2 and (c) EVCS 3.

IV. Conclusion

This work introduced a two-layer grid-aware hierarchical MPC framework for real-time coordination of colocated EVCSs on distribution systems. The key innovation lies in integrating an NSSM for capturing nonlinear feeder dynamics with a proportional load-sharing mechanism that equitably distributes available feeder capacity among colocated EVCSs. This combination allows the UL-MPC to preserve grid awareness by enforcing voltage and thermal constraints while autonomously distributing capacity to each EVCS. Concurrently, each LL-MPC optimizes local charging based on PV generation, BESS flexibility, and TOU pricing, ensuring user objectives are met within the UL-MPC's permitted import limits. Unlike existing distributed MPC or price-based methods that rely on linearized models or deterministic forecasts, the proposed hierarchical control captures nonlinear feeder responses and adapts to stochastic EV behavior, enabling scalable, privacy-preserving, and fair coordination of EVCSs. Simulation results on the IEEE 69-bus feeder demonstrate that the proposed framework reduces feeder peak loading by 34%, limits colocated EVCS peaks by up to 70%, and maintains voltage and thermal compliance across all operating conditions.

References

[1] R. K. Gupta, S. Fahmy, M. Chevron, R. Vasapollo, E. Figini, and M. Paolone, "Grid-aware scheduling and control of electric vehicle charging stations for dispatching active distribution networks: Theory and experimental validation," *IEEE Transactions on Smart Grid*, vol. 16, no. 2, pp. 1575–1589, 2025.

[2] M. Sarkhosh and A. Fattahi, "Network-aware electric vehicle charging/discharging scheduling for grid load management in a hierarchical framework," *Computers and Electrical Engineering*, vol. 121, p. 109903, 2025.

[3] H. T. Nguyen and D.-H. Choi, "Decentralized distributionally robust coordination between distribution system and charging station operators in unbalanced distribution systems," *IEEE Transactions on Smart Grid*, vol. 14, no. 3, pp. 2164–2177, 2023.

[4] K. Li, C. Shao, M. Shahidehpour, and X. Wang, "A capacity-based regulation method for coordinating electric vehicle charging flows in coupled distribution and transportation networks," *IEEE Transactions on Smart Grid*, vol. 15, no. 3, pp. 3066–3079, 2024.

[5] D. Yan and Y. Chen, "A distributed online algorithm for promoting energy sharing between EV charging stations," *IEEE Transactions on Smart Grid*, vol. 14, no. 2, pp. 1158–1172, 2023.

[6] R. Ramaschi, S. Polimeni, A. Cabrera-Tobar, and S. Leva, "Two-layer optimization approach for electric vehicle charging station with dynamic reconfiguration of charging points," *Sustainable Energy, Grids and Networks*, vol. 40, p. 101531, 2024.

[7] Z. Ullah, L. Yan, A. U. Rehman, H. S. Qazi, W. Xiaodong, L. Jingkuan, and H. M. Hasanien, "Distributed consensus-based optimal power sharing between grid and EV charging stations using derivative-free charging scheduling," *IEEE Access*, vol. 12, pp. 127 768–127 781, 2024.

[8] H. Saber, H. Ranjbar, E. Hajipour, and M. Shahidehpour, "Two-stage coordination scheme for multiple EV charging stations connected to an exclusive DC feeder considering grid-tie converter limitation," *IEEE Transactions on Transportation Electrification*, vol. 10, no. 4, pp. 8213–8223, 2024.

[9] A. S. Abdelaal and R. ElShatshat, "Towards net-zero emission in hybrid power microgrids: A data-driven MPC-based optimization approach," in *2025 IEEE Power & Energy Society General Meeting (PESGM)*, 2025, pp. 1–5.

[10] Ontario Energy Board, "Electricity Rates," 2025, accessed: 2026-01-23. [Online]. Available: https://www.oeb.ca/consumer-information-and-protection/electricity-rates

[11] R. P. Upputuri and B. Subudhi, "A comprehensive review and performance evaluation of bidirectional charger topologies for V2G/G2V operations in EV applications," *IEEE Transactions on Transportation Electrification*, vol. 10, no. 1, pp. 583–595, 2024.

[12] A. Verdone, M. Panella, E. De Santis, and A. Rizzi, "A review of solar and wind energy forecasting: From single-site to multi-site paradigm," *Applied Energy*, vol. 392, p. 126016, 2025.

[13] A. Ul-Haq, C. Cecati, and E. El-Saadany, "Probabilistic modeling of electric vehicle charging pattern in a residential distribution network," *Electric Power Systems Research*, vol. 157, pp. 126–133, 2018.

979-8-3315-8138-1